

Consistent-1-to-3: Consistent Image to 3D View Synthesis via Geometry-aware Diffusion Models

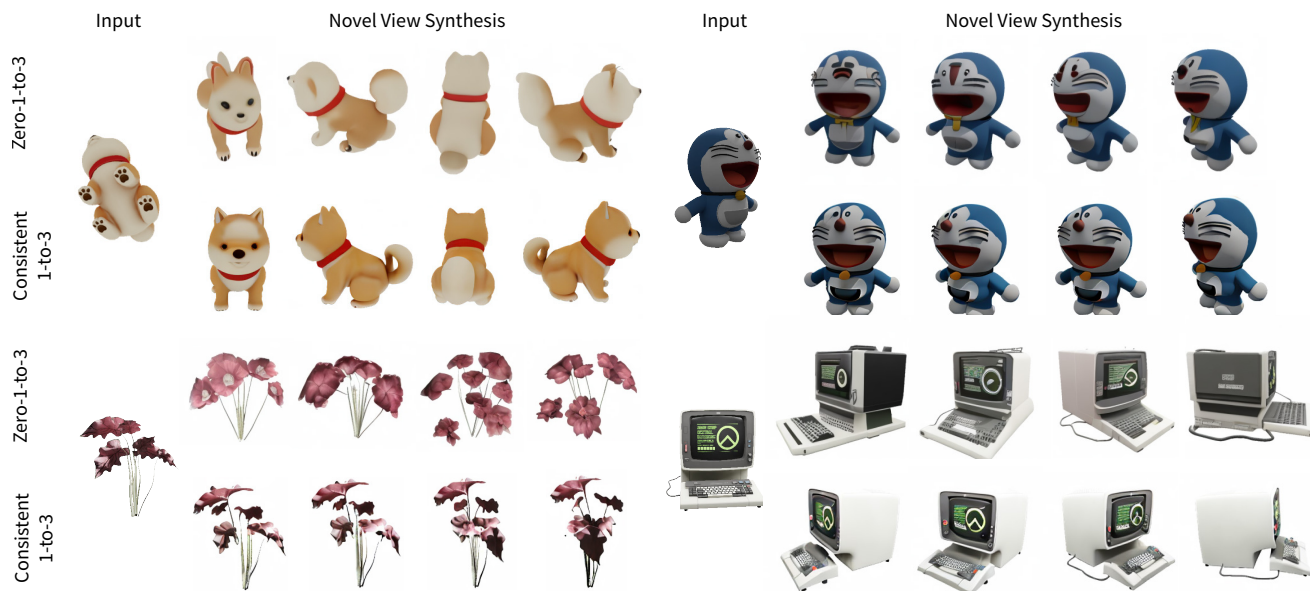
Jianglong Ye¹Peng Wang²Kejie Li²Yichun Shi²Heng Wang²¹UC San Diego²ByteDance

Figure 1. **Consistent-1-to-3** is a novel framework that generates consistent images of any objects from any viewpoint given a single image.

Abstract

Zero-shot novel view synthesis (NVS) from a single image is an essential problem in 3D object understanding. While recent approaches that leverage pre-trained generative models can synthesize high-quality novel views from in-the-wild inputs, they still struggle to maintain 3D consistency across different views. In this paper, we present **Consistent-1-to-3**, which is a generative framework that significantly mitigates this issue. Specifically, we decompose the NVS task into two stages: (i) transforming observed regions to a novel view, and (ii) hallucinating unseen regions. We design a scene representation transformer and view-conditioned diffusion model for performing these two stages respectively. Inside the models, to enforce 3D consistency, we propose to employ epipolar-guided attention to incorporate geometry constraints, and multi-view attention to better aggregate multi-view information. Finally, we design a hierarchy generation paradigm to generate long sequences of consistent views, allowing a full 360° observation of the provided object image. Qualitative and quantitative evaluation over multiple datasets

demonstrates the effectiveness of the proposed mechanisms against state-of-the-art approaches. Our project page is at <https://jianglongye.com/consistent123/>.

1. Introduction

Synthesizing high-quality and visually consistent novel views of real-world objects from a single input image has been a long-standing problem in computer vision. Its applications are widespread, ranging from content creation [20, 33], robotic manipulation and navigation [29], to AR/VR [16].

This task is challenging as it involves difficulties from both reconstruction and generation, which require not only accurate geometry transformation of observed parts but also hallucination of unseen regions. In recent years, the field has seen significant progress with the advance of large-scale data-driven deep 2D models. For example, transformer models for single view reconstruction, e.g., DPT [35], GANs [11] and 2D diffusion models for image generation [8].

To tackle such a challenge, one set of works requires a time-consuming iterative optimization to obtain novel view

	Single instance					Re-projection					Latent			Diffusion					Ours			
	NeRF [28]	RegNeRF [31]	VolSDF [56]	RealFusion [25]	3D Fuse [41]	IBRNet [51]	PixelNeRF [57]	NerFormer [36]	GPNR [46]	VisionNeRF [19]	HumanVE [61]	PetNVS [43]	LFN [45]	SRT [39]	OSRT [38]	3DIM [52]	SparseFusion [60]	NerDiff [12]	GeNVS [2]	Zero-1-to-3 [22]	Consistent-1-to-3	
1) Single-view	×	×	×	✓	✓	×	✓	✓	×	✓	×	×	×	×	×	✓	×	✓	✓	✓	✓	✓
2) Sparse-views (2-4)	×	✓	✓	✓	✓	×	✓	✓	×	✓	×	×	×	✓	✓	✓	×	✓	✓	✓	✓	✓
3) Multi-view consistent	✓	✓	✓	✓	✓	✓	✓	✓	✓	✓	✓	✓	✓	✓	✓	✓	✓	✓	✓	×	✓	✓
4) Generate unseen	×	×	×	✓	✓	×	×	×	×	×	✓	×	×	×	×	✓	✓	✓	✓	✓	✓	✓
5) Open-set generalization	×	×	×	✓	✓	×	×	×	×	×	×	×	×	×	×	×	×	×	×	✓	✓	✓
6) Train-free for new instances	×	×	×	×	×	✓	✓	✓	✓	✓	✓	✓	✓	✓	✓	✓	✓	✓	✓	✓	✓	✓

Table 1. **Comparison with prior methods.** The rows indicate whether each method: 1) works with a single input view, 2) works with sparse (2-4) input views, 3) generate consistent multiple views, 4) hallucinates unseen regions, 5) generalizes to open-set instances instead of limited categories, 6) free of time-consuming training for new instances. Our proposed method stands out as the only approach that possesses all these advantages.

images through building an object-specific model such as RealFusion [25], NeuralLift [55] and SSDNerf [34], where the input image needs to be involved in a multi-round training process. We note them as training-based methods. Another set of works targets fast and efficient synthesis, which can complete the task with a single forward process of the given image, *e.g.*, MCC [53], Graf [40] and Zero123 [22]. We note them as training-free methods. In this paper, our method falls into the second category since more efficiency implies a wider range of applications. In principle, the effectiveness and generalization of training-free methods come from using a deep network to learn the prior information from a sufficiently large amount of 2D/3D data. For example, one may adopt large transformers [36, 53] or diffusion-based models [2, 22] for view synthesis.

Among training-free methods, we are particularly interested in Zero123 [22], since it is among the recent models that can produce SoTA NVS quality, and generalize well to out-of-distribution images. We will discuss other models in related works in Sec. 2. Specifically, Zero123 finetunes a pre-trained image-to-image diffusion model [1] on a large CAD dataset [7] with a novel camera embedding condition in the diffusion model. Although the quality is impressive, as shown in the top rows of Fig. 1, we found the results are still not geometrically consistent. While we conjecture this issue could be largely mitigated if given enough training data such as 10x bigger than objaverse-XL [6] and adopted even larger pre-trained models such as Stable-Diffusion-XL [32], the current model for NVS is still resource-constrained, and the architecture design is essential for the quality of synthesized images.

Therefore, we take a further step towards architecture optimization by designing a model that handles the challenges from reconstruction and generation separately, which significantly improves the geometric consistency, as shown in the bottom rows of Fig. 1. To motivate our architecture

design, we did an in-depth study of the Zero123 model, and concluded that the inconsistency comes from the inherent uncertainty of the diffusion-based model where a non-deterministic process is performed given a noisy input. Therefore, it is difficult to maintain the 3D consistency across independently sampled views. To tackle this issue, we introduce a two-stage model, as shown in Fig. 2. In the first stage, we set up a deterministic Scene Representation Transformer (SRT) [39] which quickly transforms the observed image into novel views that roughly represent the object’s shape and appearance. In the second stage, we design a view-conditioned diffusion model, which is conditioned not only on the camera embedding but also the outputs from SRT, to produce clear and detailed images for unseen regions. To enforce 3D consistency, we additionally employ epipolar-guided attention [48] and multi-view attention [42] to better aggregate multi-view information. Finally, a hierarchy generation paradigm is proposed to generate long sequences of consistent 3D views, allowing a full experience of 360° observation of the provided object image. We name this architecture as Consistent 1-to-3 and experiment with it over several popular datasets [7]. In all cases, our results outperform other SoTA methods in terms of both quality and consistency, demonstrating the effectiveness of the proposed method. Finally, Consistent 1-to-3 can further improve the NVS performance when using few-shot images as input.

In summary, our paper contributes a novel geometric-aware deep model, namely Consistent 1-to-3, for efficient novel view synthesis. With extensive experiments on multiple datasets, it produces state-of-the-art synthesis quality and geometric consistency across various camera viewpoints.

2. Related Work

In this section, we briefly review the literature in novel-view synthesis and group related methods based on their attributes,

shown in Tab. 1. In the following, we will walk through these works on NVS to show the uniqueness of Consistent 1-to-3. We recognize the breadth and diversity within NVS, and only include representative works due to limited space. While we acknowledge the existence of other significant contributions, citing them all is beyond our scope.

Single Instance Training-based Reconstruction. As discussed in Sec. 1, this thread of works introduces a multi-round optimization strategy to obtain an instance-specific model for view synthesis. NeRF [27] first proposes a neural network that optimizes around 100 images to produce realistic synthesized images. VolSDF [56] can train a NeRF model with tens of images by incorporating a 3D volume representation. Later works try to further reduce the number of required images, while maintaining the original rendering quality. RegNeRF [31] takes 3 images and adopts a geometry loss from depth patches. SinNerf [54], RealFusion [25] and NeuralLift [55] further reduce the required images to a single one by combining either depth map or Score Distillation Sampling [33] during the nerf model training. However, all these strategies need time-consuming optimization, *e.g.*, more than 30 mins for a single model for RealFusion, which hinders a wide range of interactive applications.

Re-projection methods. This thread of works considers adopting an explicit geometry representation, then doing a 3D re-projection for novel view synthesis. IBRNet [50] and GPNR [46] adopts image-based view synthesis using a sparse set of nearby views with pixel or patch-based embedding. PixelNeRF [57] trained a generalizable Nerf model with 13 object categories from ShapeNet [3] while not showing its ability to learn from large amount of instances in open-set images such as Objaverse [7]. NerFormer [36] further enlarges the 3D datasets to 50 categories with 18,619 instances and proposes a transformer for view synthesis from a small number of images. Later, MCC [53] introduce a volume representation yielding better performance when a single image is given, but the rendered images lack details. In addition to category-agnostic approaches, some works adopt category-specific mesh models as prior to improve the results such as Human View Extrapolation (HumanVE) [61] or Pet Novel View Synthesis (PetNVS) [43]. These models can hardly generalize to open-set instances.

Latent methods. This thread of work generalizes the explicit pixel representation to latent ones and learns MLP to directly decode the latent code to novel-view rather than performing ray aggregation from NeRF, yielding much faster rendering speed. This is first proposed in LFN [45]. Later, SRT [39] further reduced the necessary observed images to a few shots. However, these methods have not shown their generalization ability across open-set categories.

Diffusion Models for NVS. This thread of work extends existing image diffusion models to conditional diffusion models where input views and target camera parameters are

used as the conditions for generating a target view. Watson *et al.* [52] first proposed to use diffusion models for such a task by training a diffusion model on the SRN ShapeNet dataset [44]. SparseFusion [60] combines stable diffusion model [37] with epipolar feature transformer for a view-conditioned diffusion model in the latent space. GeNVS [2] proposed to improve the view consistency of the diffusion model by re-projecting the latent feature of input view before diffusion denoising. However, all of these works are limited to their training data and have not been proven to generalize to arbitrary image input. Zero-1-to-3 [22] utilizes pre-trained stable diffusion model [1] and fine-tunes it on a large 3D render dataset. It is found that such a fine-tuned model is able to generate high-quality novel view output with relatively good generalizability compared to prior works. The follow-up work One-2-3-45 [21] takes advantage of the generalization capabilities of Zero-1-to-3 and employs a feed-forward network to obtain a mesh representation. More recently, MV-Dream [42] proposes a similar multi-view diffusion mechanism to generate geometrically consistent multi-view images from a given text prompt.

3D Diffusion Models. Utilizing categorical 3D datasets, numerous works have leveraged diffusion models directly on 3D shapes. Zhou *et al.* [59] and Zeng *et al.* [49] employ diffusion models for 3D point clouds. PC^2 [26] learns a point cloud generation model conditioned on a single image. Diffusion models based on various 3D representations, such as meshes [23], volumes [4], and neural implicit representations [5, 13], have also been explored. We have also seen rapid progress on the more challenging open-set (or universal) 3D generation [58] thanks to the release of Objaverse [7], a large-scale 3D model repository. Researchers from OpenAI also proposed Point-e [30], and Shap-e [15] for open-set 3D generation conditioned on texts or images using internal 3D datasets.

3. Method

Given a single observation of an object, denoted as $\mathbf{x}^{\text{source}}$, with known camera parameters π^{source} , our goal is to synthesize a set of multi-view consistent images using target camera parameters π^{target} . As illustrated in Fig. 2, our pipeline consists of two key components: 1) A Scene Representation Transformer that learns a latent 3D representation given a single view; and 2) a view-conditioned diffusion model to capture the generative aspects of novel view synthesis. We first detail the pipeline in Sec. 3.1, and introduce several essential techniques to further enhance multi-view consistency in Sec. 3.2. Lastly, we extend the proposed Novel View Synthesis pipeline to facilitate 3D reconstruction (Sec. 3.3).

3.1. Geometry-guided Novel View Synthesis

We decompose the NVS task into two sub-tasks: (i) photometric warping, which is guided by epipolar constraints to

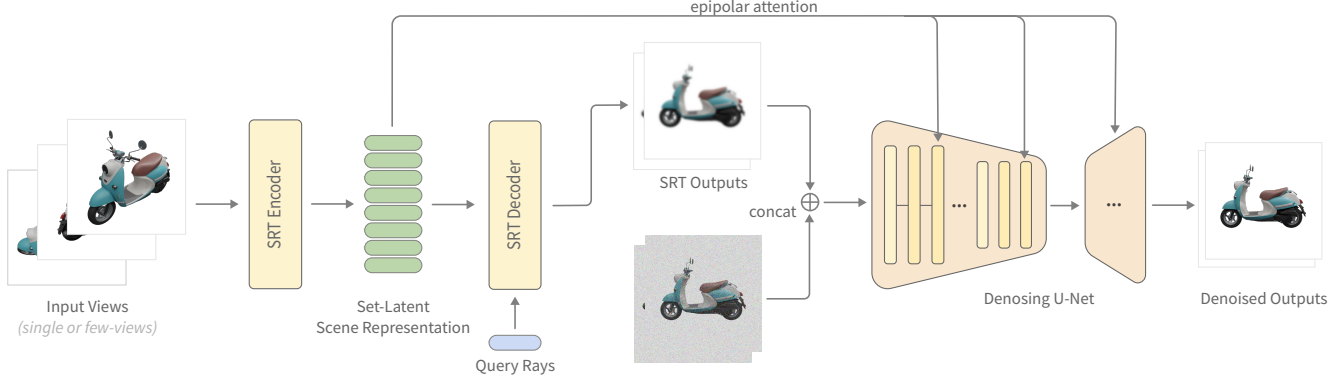


Figure 2. **Pipeline of Consistent-1-to-3.** Given a single or a sparse set of input images, the encoder within Scene Representation Transformer (SRT) translates the image(s) into latent scene representations, effectively capturing implicit 3D information. The image rendering unfolds in two stages. The initial stage produces a rough yet geometry-grounded output by cross-attending the queried pixels to the latent scene representation. Subsequently, these intermediate outputs are taken as input by the view-conditioned diffusion model, resulting in visually appealing images that exhibit consistency among the input and generated images from different viewpoints.

ensure accurate alignment of observed regions, and (ii) hallucination of unseen regions based on observed regions. To accomplish these sub-tasks, we utilize a scene representation transformer for photometric warping and a view-conditioned diffusion model for the generation of unseen regions.

Scene Representation Transformer (SRT). SRT [39] builds upon a transformer encoder-decoder architecture to learn an implicit 3D representation given a set of posed images $(\mathbf{x}^{\text{source}}, \boldsymbol{\pi}^{\text{source}})$:

$$\mathbf{z} = f_e \circ f_c(\mathbf{x}^{\text{source}}, \boldsymbol{\pi}^{\text{source}}), \quad (1)$$

where a CNN backbone f_c extracts patch-level features from posed input images and feeds them as tokens to the transformer encoder f_e . The encoder converts input tokens to a set-latent scene representation \mathbf{z} via self-attention.

To render a novel image of the scene represented by \mathbf{z} , the decoder of SRT queries the pixel color via cross attention between the ray corresponding to the pixel $\mathbf{r} \equiv (\mathbf{o}, \mathbf{d})$ with \mathbf{o} and \mathbf{d} being the origin and normalized direction of the ray and the set-latent scene representation \mathbf{z} :

$$\hat{C}(\mathbf{r}) = f_d(\mathbf{r}, \mathbf{z}), \quad (2)$$

where f_d is the decoder of SRT.

Several changes are necessary to integrate SRT into our pipeline. Specifically, we replace all standard attention layers with epipolar attention, which allows the model to incorporate important geometry biases (details explained below). Furthermore, we train the SRT in the image latent space, so that it not only reduces computation costs but also ensures seamless compatibility with the latent diffusion model.

Our SRT is trained by minimizing a pixel-level reconstruction loss:

$$\mathcal{L}_{\text{recon}} = \sum_{\mathbf{r} \in \mathcal{R}} \left\| C(\mathbf{r}) - \hat{C}(\mathbf{r}) \right\|_2^2, \quad (3)$$

where $C(\mathbf{r})$ is the ground truth color of the ray and \mathcal{R} is the set of rays sampled from target views.

View-conditioned Diffusion. While SRT is able to learn geometry correspondence via the attention mechanism, the pixel-level reconstruction loss leads to averaging out fine-grained details in the images, thus often resulting in blurred predictions. To capture the probabilistic nature of novel view synthesis (for the unseen parts), we employ a view-conditioned diffusion model to estimate the conditional distribution of the target view given the source view and the relative camera pose: $p(\mathbf{x}^{\text{target}} | \boldsymbol{\pi}^{\text{target}}, \mathbf{x}^{\text{source}}, \boldsymbol{\pi}^{\text{source}})$. Note that although we follow LDM [37] to perform the diffusion process in the image latent space, we still denote the image in latent space with \mathbf{x} for simplicity.

To achieve conditional generation, our denoising network ϵ_θ operates under two conditions. Firstly, the SRT predicts a 32×32 latent image $\tilde{\mathbf{x}}^{\text{target}}$ based on the target view $\boldsymbol{\pi}^{\text{target}}$. This predicted latent image is concatenated with the noisy image \mathbf{y} and fed into the denoising network. Secondly, the denoising network is also conditioned on the scene representation \mathbf{z} through multiple cross-attention layers. By incorporating these two conditions, the denoising network can effectively leverage both the target view information and the scene representation to produce sharp and realistic images that are also consistent with the input images. Concretely, the predicted images $\hat{\epsilon}_t$ are given by:

$$\hat{\epsilon}_t = \epsilon_\theta(\mathbf{y}, \tilde{\mathbf{x}}^{\text{target}}, \mathbf{z}, t), \quad (4)$$

where t is the timestep.

The network is trained by optimizing a simplified variational lower bound:

$$\mathcal{L}_{\text{diffusion}} = \mathbb{E} \left[\left\| \epsilon_t - \epsilon_\theta(\mathbf{y}, \tilde{\mathbf{x}}^{\text{target}}, \mathbf{z}, t) \right\|^2 \right] \quad (5)$$

Epipolar Attention. While previous works on the view-conditioned diffusion model [22] employ full attention in

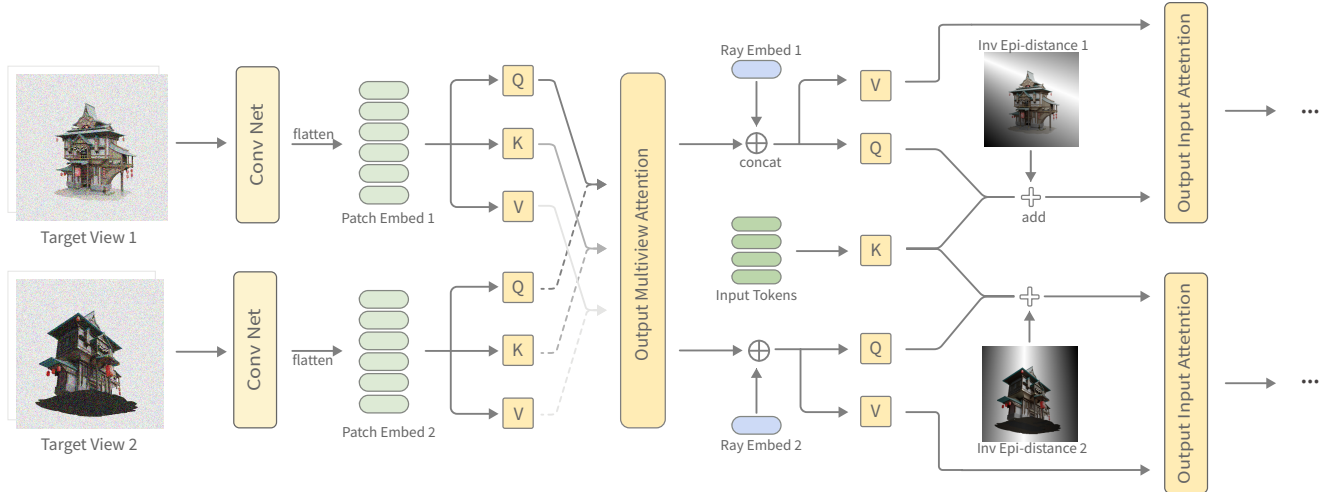


Figure 3. **Details of UNet Block.** After image features are extracted by CNN, they are aggregated via the multi-view attention mechanism in the transformer. The output images are conditioned on 1) the multi-view feature; 2) the queried ray; and 3) the affinity matrix reweighted by the epipolar attention.

their model, we propose to exploit the valuable information between images through relative camera poses using epipolar constraints. To this end, we replace all cross-attention layers in our SRT and diffusion model between source and target views with our novel epipolar attention mechanism. In our implementation of epipolar attention, we reweigh the affinity matrix $A_{i,j}$ between the i^{th} and j^{th} view by taking the epipolar distance into account. For each pixel in view i , we compute the epipolar line in view j and determine the epipolar distance for all pixels in view j . Subsequently, we convert the inverse epipolar distance into a weight map $K_{i,j}$. The affinity matrix is then reweighted using $A'_{i,j} = A_{i,j} + K_{i,j}$.

3.2. Improving Multi-view Consistency

To generate smooth Novel View Synthesis (NVS) images, it is essential to ensure not only the consistency between the generated views and input view but also the consistency among the generated views themselves. While our novel pipeline mentioned earlier primarily emphasizes the consistency between generated and input views, we introduce additional beneficial techniques to enhance the consistency among the generated views. These techniques are designed to further improve the quality and coherency of the synthesized views, providing more visually pleasing and accurate images.

Multi-view Attention. In contrast to previous methods, such as Zero123 [22], which generate multiple images of a given object instance sequentially, we have observed that this sequential approach can introduce inconsistencies between generated views due to randomness in the multiple backward passes of the diffusion model. To address this issue, we propose an alternative approach to learn the joint distribution of multi-view images. This means predicting several

novel views simultaneously given the source image x^{source} . To achieve this, as demonstrated in Fig. 3, we modify the UNet architecture by feeding a batch of noisy multi-view images during the forward pass and extending the self-attention block to work with multi-view images such that information of different viewpoints is aggregated to produce consistent rendered images.

Hierarchy Generation. To generate novel views that are far from the input viewpoint, one naive approach is to generate the target view directly. Nonetheless, this approach is less effective due to self-occlusion that caused unreliable epipolar matching. Instead, we present a hierarchical approach for generating extensive sequences of novel views. Specifically, we generate new images conditioned on not only the input view but also previously generated views.

3.3. 3D Reconstruction

While consistent NVS is great for 3D assets preview and many other applications, many scenarios within AR/VR still require accurate 3D objects for occlusion/lighting reasoning that is attributed to realistic and immersive experience.

Following Zero123 [22], we adopt an optimization-based method to generate 3D assets using Score Distillation Sampling (SDS) [33]. The fundamental concept behind SDS optimization involves updating the 3D representation, often in the form of a NeRF model, by maximizing the likelihood of rendered views using a trained 2D diffusion model. When applying our model to the SDS optimization process, we sample a set of random camera poses instead of a single one to accommodate the multi-view attention mentioned earlier.

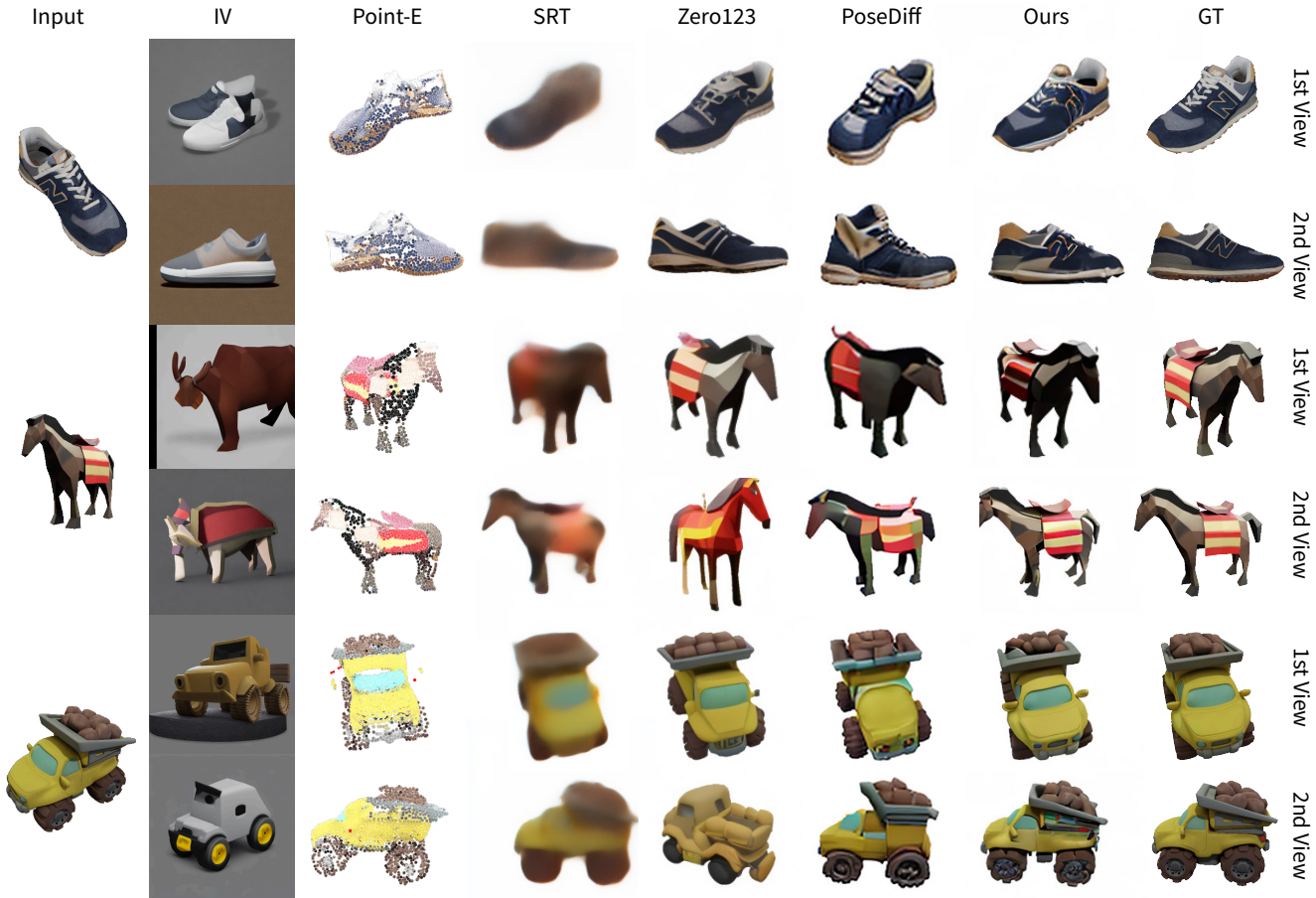


Figure 4. **NVS visualization.** We visualize the NVS results across a wide range of methods on the Objaverse dataset. Our approach outperforms the competitive baselines by producing both realistic and consistent images.

4. Experiments

4.1. Experimental Setting

Dataset. We fine-tune our diffusion model on the recently released Objaverse [7] dataset, which is a large-scale CAD dataset containing 800K high-quality objects. We directly employ the processed rendering data from Zero123, which provides 12 random views for each object. For evaluation, we use the test split of Objaverse provided by Zero123. In addition, to test our model’s performance on the out-of-distribution data, we also evaluate on the Google Scanned Objects [10] dataset, which contains high-quality scanned household items. Images in all datasets are resized to 256×256 . The background is set to white.

Metrics. Following previous works [22], we use Peak signal-to-noise ratio (PSNR), Structural Similarity Index (SSIM), and Learned Perceptual Image Patch Similarity (LPIPS) to measure the similarity between rendered images and ground truth images. Moreover, we use the flow warping error E_{warp} [17] to quantify the consistency across different

views. Specifically, we generate a 32-frame video along a pre-defined circle of camera trajectory for each object and then use the RAFT model [47] to compute the optical flow between two consecutive generated frames. The error E_{warp} is defined as

$$E_{\text{warp}} = \sum_i \left\| \mathbf{x}^i - \hat{\mathbf{x}}^{i-1} \right\|_1,$$

where $\hat{\mathbf{x}}^{i-1}$ is warped from the generated frame \mathbf{x}^{i-1} using the optical flow.

Baselines. We mainly evaluate our approach against methods that can generalize to open-set categories and accept single-view RGB images as inputs. In particular, we measure our performance against Zero123 [22], the first work that fine-tune the view-conditioned diffusion model on Objaverse, showcasing impressive zero-shot ability. Following Zero123, we also report results of Image Variation [1], a Stable Diffusion model conditioned on images, which is also the pre-trained model we fine-tuned from. Besides, we adapt Pose-Guided Diffusion [48], a recent diffusion model

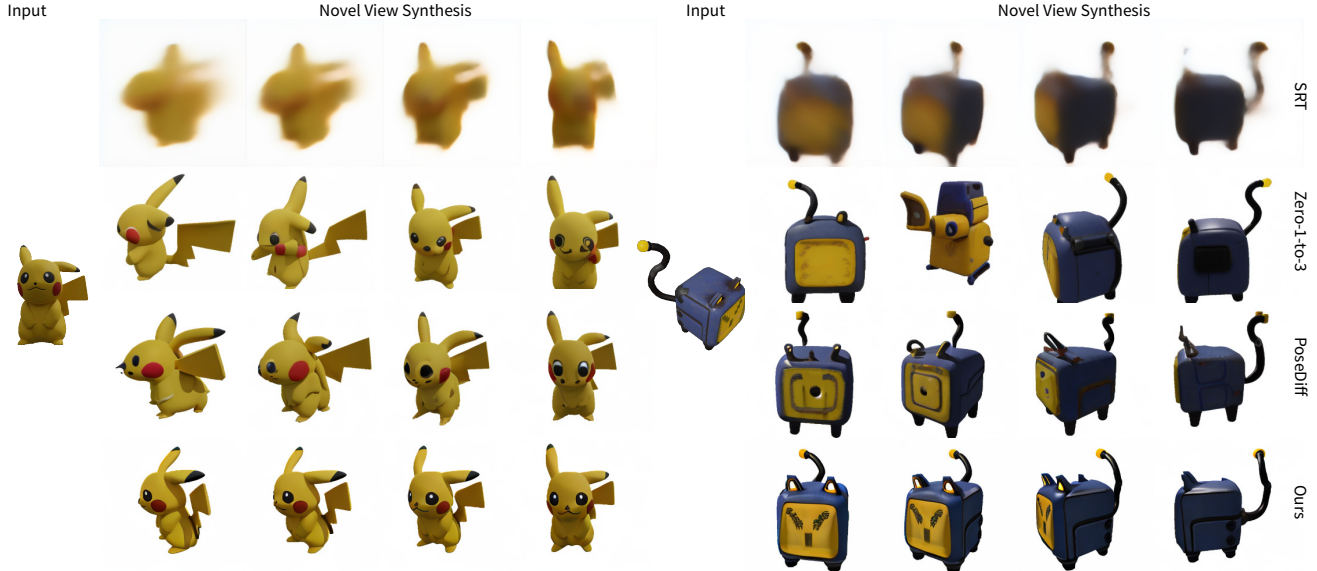


Figure 5. **Qualitative results on NVS Consistency.** While SRT (the first row) can generate views that are geometrically consistent with the input image, the rendered images are blurry. Previous diffusion-based approaches (the second and third row) are able to generate sharp and realistic-looking images, but the diffusion process leads to inconsistency. Our geometry-guided approach gets the best of both worlds, generating not only plausible but also consistent images.

	↑ PSNR	↑ SSIM	↓ LPIPS	↓ E_{warp}
ImageVariation [1]	6.42	0.506	0.578	22.4
Zero-1-to-3 [22]	18.13	0.828	0.157	14.2
Pose-Diffusion* [48]	18.92	0.841	0.141	7.0
Ours	20.72	0.877	0.112	3.7

Table 2. **Quantitative results on Objaverse.** We evaluate our method on the test split of Objaverse and demonstrate significant improvements across all metrics. Pose-Diffusion* is our re-implemented version.

for generating consistent videos using an epipolar attention mechanism similar to ours. Since the code wasn’t public, we re-implement and re-train it on Objaverse. We also add a camera embedding the same as ours to the model for more precise view control.

Implementation Details. Both SRT encoder and decoder are adapted from ViT-Base [9]. In encoder, the attention layers has 12 heads and 4 layers, the decoder’s attention layers consist of 6 heads and 3 layers. The ray for each image patch is parameterized in Plucker coordinates [45] and the dimension of ray embedding is 120. The MLPs in SRT have 1 hidden layer and GELU activations [14]. The VAE modules in diffusion models are frozen during training. The downsample scale of VAE is 8, which results in 32×32 latent images. The basic UNet module is borrowed from Stable Diffusion. We use AdamW [24] with a learning rate of 5×10^{-5} for training. The model is fine-tuned with a batch size of 1024 on $32 \times A100-80GB$ for 7 days.

	↑ PSNR	↑ SSIM	↓ LPIPS	↓ E_{warp}
ImageVariation [1]	5.93	0.538	0.529	19.9
Zero-1-to-3 [22]	16.72	0.721	0.212	11.7
Pose-Diffusion* [48]	17.52	0.791	0.174	5.2
Ours	19.46	0.858	0.146	3.3

Table 3. **Quantitative results on Google Scanned Objects.** Evaluation of novel-view synthesis on the out-of-distribution GSO dataset. Ours is best across datasets and metrics.

4.2. Novel View Synthesis

We present quantitative results for NVS on both in-distribution and out-of-distribution datasets in Tab. 2 and 3. Our proposed mechanisms significantly improve the performance of all metrics. Fig. 4 shows a comparison of NVS results on Objaverse with our method and all baselines. The SRT [39] results are obtained by training the SRT part of our model with only the reconstruction loss. On one side, Point-E and SRT fail to produce realistic images but remain consistent with the input; on the other side, diffusion-based baselines (Zero123 and PoseDiff) can generate realistic images but do not align well with the ground truth. Our approach is the only one that achieves both fidelity and consistency.

Fig. 5 provides the qualitative results for the NVS consistency. We render a sequence of images using the same camera trajectory for each approach. While previous diffusion models (Zero123 and PoseDiff) are able to generate realistic novel views, they often suffer from inconsistent issues across the independently sampled views. By incorpo-

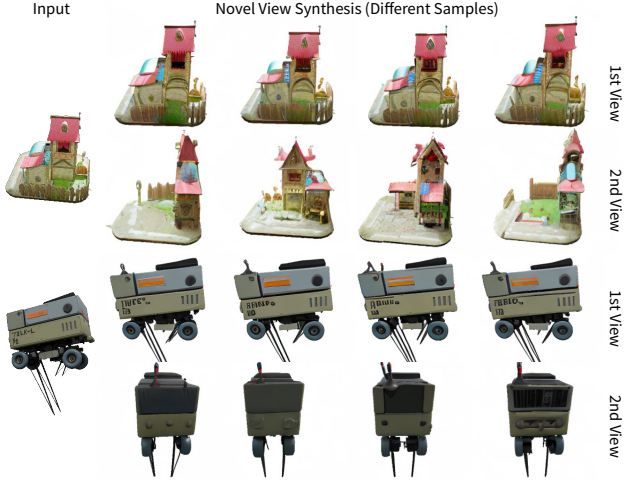


Figure 6. **Diversity of NVS results.** Nearby views (the 1st view) maintain consistency with the input image, while distant views (the 2nd view) generate a variety of expressive yet realistic images. Note the diverse patterns on the back of the trailer.

	\uparrow PSNR	\uparrow SSIM	\downarrow LPIPS	$\downarrow E_{warp}$
w.o. epi attention	19.34	0.847	0.148	4.3
w.o. in-out attention	18.79	0.823	0.156	4.6
w.o. mv-out attention	20.84	0.879	0.120	7.0
w.o. hierarchy generation	21.03	0.883	0.107	8.8
full model	20.72	0.877	0.112	3.7

Table 4. **Ablation study on Objaverse.** Each of our design choices contributes to fidelity or consistency. Refer to the text for the detailed discussion.

rating epipolar constraint and modeling the joint distribution of multi-views, our method significantly alleviates this issue.

By learning the data distribution, diffusion approaches, by nature, can generate more diverse samples. But when dealing with NVS tasks, observed regions in target views must reflect the geometric transformation rather than being randomly generated. Our design is guided by this motivation, and Fig. 6 shows the effectiveness of our design. The first view of each object is close to the input view, and all generated images align with the input. But for the unseen regions shown in the second view, the variation of generated images is much larger than the first view.

4.3. 3D Reconstruction

Fig. 7 qualitatively shows the 3D reconstruction results of our method. For each instance, we optimize a NeRF via the SDS loss, the colored images in the figure are all NeRF renderings. After reconstructing NeRFs, we further utilize DiffRast [18] to extract meshes from NeRFs. In this way, we leverage the multi-view prior from our diffusion models and combine them with the advanced NeRF-style reconstruction.

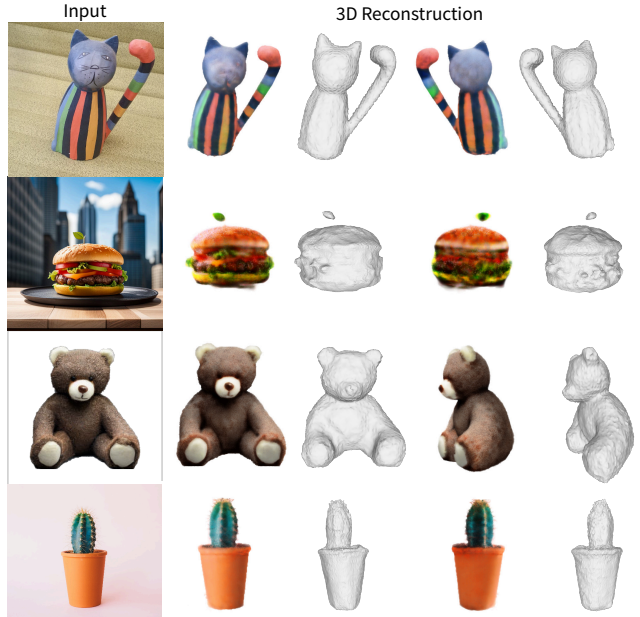


Figure 7. **3D reconstruction.** By combining the view-conditioned diffusion model and NeRF-style reconstruction techniques, our method is able to perform high-fidelity 3D reconstruction for any single image.

4.4. Ablation Study

We ablate each design choice in our method and present quantitative results in Tab. 4. The epipolar line guidance (1st row) and the attention between inputs and outputs (2nd row) enforce the model to learn the better geometric transformation of observed regions in source views, and thus they are essential to the similarity metrics (PSNR, SSIM, and LPIPS). The attention between multiple outputs (3rd row) and the hierarchy generation (4th row) contributes a lot to the consistency across different views. However, it should be noted that these two mechanisms will slightly hurt the reconstruction performance, and our full model is a trade-off between fidelity and consistency.

5. Conclusion

In this paper, we proposed Consistent 1-to-3, a geometry-aware deep model that produces high quality and 3D consistent novel view synthesis from a single image or few-shot images. Consistent 1-to-3 is a two-stage model that first uses a transformer to generate a blurry while geometry correct image, and then uses a diffusion model to finish the details. We demonstrate by following such a generation progression, the generated results are significantly improved. We hope our work could motivate future studies on incorporating better geometry constraints and representations inside the model, which could significantly improve its practical usage.

References

- [1] Stable diffusion image variations - a hugging face space by lambdalabs. [2](#), [3](#), [6](#), [7](#)
- [2] Eric R. Chan, Koki Nagano, Matthew A. Chan, Alexander W. Bergman, Jeong Joon Park, Axel Levy, Miika Aitala, Shalini De Mello, Tero Karras, and Gordon Wetzstein. GeNVS: Generative novel view synthesis with 3D-aware diffusion models. In *arXiv*, 2023. [2](#), [3](#)
- [3] Angel X. Chang, Thomas A. Funkhouser, Leonidas J. Guibas, Pat Hanrahan, Qi-Xing Huang, Zimo Li, Silvio Savarese, Manolis Savva, Shuran Song, Hao Su, Jianxiong Xiao, L. Yi, and Fisher Yu. Shapenet: An information-rich 3d model repository. *ArXiv*, abs/1512.03012, 2015. [3](#)
- [4] Yen-Chi Cheng, Hsin-Ying Lee, Sergey Tulyakov, Alexander G Schwing, and Liang-Yan Gui. Sdfusion: Multimodal 3d shape completion, reconstruction, and generation. In *Proceedings of the IEEE/CVF Conference on Computer Vision and Pattern Recognition*, pages 4456–4465, 2023. [3](#)
- [5] Gene Chou, Yuval Bahat, and Felix Heide. Diffusionsdf: Conditional generative modeling of signed distance functions. *arXiv preprint arXiv:2211.13757*, 2022. [3](#)
- [6] Matt Deitke, Ruoshi Liu, Matthew Wallingford, Huong Ngo, Oscar Michel, Aditya Kusupati, Alan Fan, Christian Laforte, Vikram Voleti, Samir Yitzhak Gadre, Eli VanderBilt, Anirudha Kembhavi, Carl Vondrick, Georgia Gkioxari, Kiana Ehsani, Ludwig Schmidt, and Ali Farhadi. Objaverse-xl: A universe of 10m+ 3d objects. 2023. [2](#)
- [7] Matt Deitke, Dustin Schwenk, Jordi Salvador, Luca Weihs, Oscar Michel, Eli VanderBilt, Ludwig Schmidt, Kiana Ehsani, Anirudha Kembhavi, and Ali Farhadi. Objaverse: A universe of annotated 3d objects. In *Proceedings of the IEEE/CVF Conference on Computer Vision and Pattern Recognition*, pages 13142–13153, 2023. [2](#), [3](#), [6](#), [1](#)
- [8] Prafulla Dhariwal and Alexander Quinn Nichol. Diffusion models beat gans on image synthesis. In *Advances in Neural Information Processing Systems 34: Annual Conference on Neural Information Processing Systems 2021, NeurIPS 2021, December 6-14, 2021, virtual*, pages 8780–8794, 2021. [1](#)
- [9] Alexey Dosovitskiy, Lucas Beyer, Alexander Kolesnikov, Dirk Weissenborn, Xiaohua Zhai, Thomas Unterthiner, Mostafa Dehghani, Matthias Minderer, Georg Heigold, Sylvain Gelly, Jakob Uszkoreit, and Neil Houlsby. An image is worth 16x16 words: Transformers for image recognition at scale. In *9th International Conference on Learning Representations, ICLR 2021, Virtual Event, Austria, May 3-7, 2021*. OpenReview.net, 2021. [7](#)
- [10] Laura Downs, Anthony Francis, Nate Koenig, Brandon Kinman, Ryan Hickman, Krista Reymann, Thomas B. McHugh, and Vincent Vanhoucke. Google scanned objects: A high-quality dataset of 3d scanned household items. In *2022 International Conference on Robotics and Automation, ICRA 2022, Philadelphia, PA, USA, May 23-27, 2022*, pages 2553–2560. IEEE, 2022. [6](#)
- [11] Ian Goodfellow, Jean Pouget-Abadie, Mehdi Mirza, Bing Xu, David Warde-Farley, Sherjil Ozair, Aaron Courville, and Yoshua Bengio. Generative adversarial networks. *Communications of the ACM*, 63(11):139–144, 2020. [1](#)
- [12] Jiatao Gu, Alex Trevithick, Kai-En Lin, Joshua M Susskind, Christian Theobalt, Lingjie Liu, and Ravi Ramamoorthi. Nerfdiff: Single-image view synthesis with nerf-guided distillation from 3d-aware diffusion. In *International Conference on Machine Learning*, pages 11808–11826. PMLR, 2023. [2](#)
- [13] Anchit Gupta, Wenhan Xiong, Yixin Nie, Ian Jones, and Barlas Oğuz. 3dgen: Triplane latent diffusion for textured mesh generation. *arXiv preprint arXiv:2303.05371*, 2023. [3](#)
- [14] Dan Hendrycks and Kevin Gimpel. Gaussian error linear units (gelus). *arXiv preprint arXiv:1606.08415*, 2016. [7](#)
- [15] Heewoo Jun and Alex Nichol. Shap-e: Generating conditional 3d implicit functions. *arXiv preprint arXiv:2305.02463*, 2023. [3](#)
- [16] Johannes Kopf, Kevin Matzen, Suhil Alsison, Ocean Quigley, Francis Ge, Yangming Chong, Josh Patterson, Jan-Michael Frahm, Shu Wu, Matthew Yu, Peizhao Zhang, Zijian He, Peter Vajda, Ayush Saraf, and Michael F. Cohen. One shot 3d photography. *ACM Trans. Graph.*, 39(4):76, 2020. [1](#)
- [17] Wei-Sheng Lai, Jia-Bin Huang, Oliver Wang, Eli Shechtman, Ersin Yumer, and Ming-Hsuan Yang. Learning blind video temporal consistency. In *Computer Vision - ECCV 2018 - 15th European Conference, Munich, Germany, September 8-14, 2018, Proceedings, Part XV*, pages 179–195. Springer, 2018. [6](#)
- [18] Samuli Laine, Janne Hellsten, Tero Karras, Yeongho Seol, Jaakko Lehtinen, and Timo Aila. Modular primitives for high-precision differentiable rendering. *ACM Transactions on Graphics*, 39(6), 2020. [8](#)
- [19] Kai-En Lin, Yen-Chen Lin, Wei-Sheng Lai, Tsung-Yi Lin, Yichang Shih, and Ravi Ramamoorthi. Vision transformer for nerf-based view synthesis from a single input image. *2023 IEEE/CVF Winter Conference on Applications of Computer Vision (WACV)*, pages 806–815, 2022. [2](#)
- [20] Yen-Chen Lin, Pete Florence, Jonathan T. Barron, Tsung-Yi Lin, Alberto Rodriguez, and Phillip Isola. Nerf-supervision: Learning dense object descriptors from neural radiance fields. In *2022 International Conference on Robotics and Automation, ICRA 2022, Philadelphia, PA, USA, May 23-27, 2022*, pages 6496–6503. IEEE, 2022. [1](#)
- [21] Minghua Liu, Chao Xu, Haiyan Jin, Ling Chen, T Mukund-Varma, Zexiang Xu, and Hao Su. One-2-3-45: Any single image to 3d mesh in 45 seconds without per-shape optimization. *ArXiv*, abs/2306.16928, 2023. [3](#)
- [22] Ruoshi Liu, Rundi Wu, Basile Van Hoorick, Pavel Tokmakov, Sergey Zakharov, and Carl Vondrick. Zero-1-to-3: Zero-shot one image to 3d object. *CoRR*, abs/2303.11328, 2023. [2](#), [3](#), [4](#), [5](#), [6](#), [7](#)
- [23] Zhen Liu, Yao Feng, Michael J Black, Derek Nowrouzezahrai, Liam Paull, and Weiyang Liu. Meshdiffusion: Score-based generative 3d mesh modeling. *arXiv preprint arXiv:2303.08133*, 2023. [3](#)
- [24] Ilya Loshchilov and Frank Hutter. Decoupled weight decay regularization. In *7th International Conference on Learning Representations, ICLR 2019, New Orleans, LA, USA, May 6-9, 2019*. OpenReview.net, 2019. [7](#)
- [25] Luke Melas-Kyriazi, Iro Laina, Christian Rupprecht, and Andrea Vedaldi. Realfusion: 360° reconstruction of any

- object from a single image. In *Proceedings of the IEEE/CVF Conference on Computer Vision and Pattern Recognition*, pages 8446–8455, 2023. 2, 3
- [26] Luke Melas-Kyriazi, Christian Rupprecht, and Andrea Vedaldi. Pc2: Projection-conditioned point cloud diffusion for single-image 3d reconstruction. In *Proceedings of the IEEE/CVF Conference on Computer Vision and Pattern Recognition*, pages 12923–12932, 2023. 3
- [27] Ben Mildenhall, Pratul P Srinivasan, Matthew Tancik, Jonathan T Barron, Ravi Ramamoorthi, and Ren Ng. Nerf: Representing scenes as neural radiance fields for view synthesis. *Communications of the ACM*, 65(1):99–106, 2021. 3
- [28] Ben Mildenhall, Pratul P. Srinivasan, Matthew Tancik, Jonathan T. Barron, Ravi Ramamoorthi, and Ren Ng. Nerf: representing scenes as neural radiance fields for view synthesis. *Commun. ACM*, 65(1):99–106, 2022. 2
- [29] Arthur Moreau, Nathan Piasco, Dzmitry Tsishkou, Bogdan Stanculescu, and Arnaud de La Fortelle. LENS: localization enhanced by nerf synthesis. In *Conference on Robot Learning, 8-11 November 2021, London, UK*, pages 1347–1356. PMLR, 2021. 1
- [30] Alex Nichol, Heewoo Jun, Prafulla Dhariwal, Pamela Mishkin, and Mark Chen. Point-e: A system for generating 3d point clouds from complex prompts. *arXiv preprint arXiv:2212.08751*, 2022. 3
- [31] Michael Niemeyer, Jonathan T. Barron, Ben Mildenhall, Mehdi S. M. Sajjadi, Andreas Geiger, and Noha Radwan. Regnerf: Regularizing neural radiance fields for view synthesis from sparse inputs. In *IEEE/CVF Conference on Computer Vision and Pattern Recognition, CVPR 2022, New Orleans, LA, USA, June 18-24, 2022*, pages 5470–5480. IEEE, 2022. 2, 3
- [32] Dustin Podell, Zion English, Kyle Lacey, Andreas Blattmann, Tim Dockhorn, Jonas Müller, Joe Penna, and Robin Rombach. Sdxl: Improving latent diffusion models for high-resolution image synthesis. *arXiv preprint arXiv:2307.01952*, 2023. 2
- [33] Ben Poole, Ajay Jain, Jonathan T. Barron, and Ben Mildenhall. Dreamfusion: Text-to-3d using 2d diffusion. In *The Eleventh International Conference on Learning Representations, ICLR 2023, Kigali, Rwanda, May 1-5, 2023*. OpenReview.net, 2023. 1, 3, 5
- [34] Siddhant Ranade, Christoph Lassner, Kai Li, Christian Haene, Shen-Chi Chen, Jean-Charles Bazin, and Sofien Bouaziz. Ssdnerf: Semantic soft decomposition of neural radiance fields. *arXiv preprint arXiv:2212.03406*, 2022. 2
- [35] René Ranftl, Alexey Bochkovskiy, and Vladlen Koltun. Vision transformers for dense prediction. In *Proceedings of the IEEE/CVF international conference on computer vision*, pages 12179–12188, 2021. 1
- [36] Jeremy Reizenstein, Roman Shapovalov, Philipp Henzler, Luca Sbordone, Patrick Labatut, and David Novotný. Common objects in 3d: Large-scale learning and evaluation of real-life 3d category reconstruction. In *2021 IEEE/CVF International Conference on Computer Vision, ICCV 2021, Montreal, QC, Canada, October 10-17, 2021*, pages 10881–10891. IEEE, 2021. 2, 3
- [37] Robin Rombach, Andreas Blattmann, Dominik Lorenz, Patrick Esser, and Björn Ommer. High-resolution image synthesis with latent diffusion models. In *IEEE/CVF Conference on Computer Vision and Pattern Recognition, CVPR 2022, New Orleans, LA, USA, June 18-24, 2022*, pages 10674–10685. IEEE, 2022. 3, 4
- [38] Mehdi S. M. Sajjadi, Daniel Duckworth, Aravindh Mahendran, Sjoerd van Steenkiste, Filip Paveti’c, Mario Luvci’c, Leonidas J. Guibas, Klaus Greff, and Thomas Kipf. Object scene representation transformer. *ArXiv*, abs/2206.06922, 2022. 2
- [39] Mehdi S. M. Sajjadi, Henning Meyer, Etienne Pot, Urs Bergmann, Klaus Greff, Noha Radwan, Suhani Vora, Mario Lucic, Daniel Duckworth, Alexey Dosovitskiy, Jakob Uszkoreit, Thomas A. Funkhouser, and Andrea Tagliasacchi. Scene representation transformer: Geometry-free novel view synthesis through set-latent scene representations. In *IEEE/CVF Conference on Computer Vision and Pattern Recognition, CVPR 2022, New Orleans, LA, USA, June 18-24, 2022*, pages 6219–6228. IEEE, 2022. 2, 3, 4, 7
- [40] Katja Schwarz, Yiyi Liao, Michael Niemeyer, and Andreas Geiger. Graf: Generative radiance fields for 3d-aware image synthesis. *Advances in Neural Information Processing Systems*, 33:20154–20166, 2020. 2
- [41] Junyoung Seo, Wooseok Jang, Minseop Kwak, Jaehoon Ko, Hyeonsu Kim, Junho Kim, Jin-Hwa Kim, Jiyoung Lee, and Seungryong Kim. Let 2d diffusion model know 3d-consistency for robust text-to-3d generation. *CoRR*, abs/2303.07937, 2023. 2
- [42] Yichun Shi, Peng Wang, Jianglong Ye, Mai Long, Kejie Li, and Xiao Yang. Mvdream: Multi-view diffusion for 3d generation. *arXiv preprint arXiv:2308.16512*, 2023. 2, 3
- [43] Samarth Sinha, Roman Shapovalov, Jeremy Reizenstein, Ignacio Rocco, Natalia Neverova, Andrea Vedaldi, and David Novotny. Common pets in 3d: Dynamic new-view synthesis of real-life deformable categories. In *Proceedings of the IEEE/CVF Conference on Computer Vision and Pattern Recognition*, pages 4881–4891, 2023. 2, 3
- [44] Vincent Sitzmann, Michael Zollhöfer, and Gordon Wetzstein. Scene representation networks: Continuous 3d-structure-aware neural scene representations. *Advances in Neural Information Processing Systems*, 32, 2019. 3
- [45] Vincent Sitzmann, Semon Rezkikov, Bill Freeman, Josh Tenenbaum, and Frédo Durand. Light field networks: Neural scene representations with single-evaluation rendering. In *Advances in Neural Information Processing Systems 34: Annual Conference on Neural Information Processing Systems 2021, NeurIPS 2021, December 6-14, 2021, virtual*, pages 19313–19325, 2021. 2, 3, 7
- [46] Mohammed Suhail, Carlos Esteves, Leonid Sigal, and Ameesh Makadia. Generalizable patch-based neural rendering. In *Computer Vision - ECCV 2022 - 17th European Conference, Tel Aviv, Israel, October 23-27, 2022, Proceedings, Part XXXII*, pages 156–174. Springer, 2022. 2, 3
- [47] Zachary Teed and Jia Deng. RAFT: recurrent all-pairs field transforms for optical flow. In *Computer Vision - ECCV 2020 - 16th European Conference, Glasgow, UK, August 23-28,*

- 2020, *Proceedings, Part II*, pages 402–419. Springer, 2020. 6, 2
- [48] Hung-Yu Tseng, Qinbo Li, Changil Kim, Suhub Alsisan, Jia-Bin Huang, and Johannes Kopf. Consistent view synthesis with pose-guided diffusion models. In *Proceedings of the IEEE/CVF Conference on Computer Vision and Pattern Recognition*, pages 16773–16783, 2023. 2, 6, 7
- [49] Arash Vahdat, Francis Williams, Zan Gojcic, Or Litany, Sanja Fidler, Karsten Kreis, et al. Lion: Latent point diffusion models for 3d shape generation. *Advances in Neural Information Processing Systems*, 35:10021–10039, 2022. 3
- [50] Qianqian Wang, Zhicheng Wang, Kyle Genova, Pratul P Srinivasan, Howard Zhou, Jonathan T Barron, Ricardo Martin-Brualla, Noah Snaveley, and Thomas Funkhouser. Ibrnet: Learning multi-view image-based rendering. In *Proceedings of the IEEE/CVF Conference on Computer Vision and Pattern Recognition*, pages 4690–4699, 2021. 3
- [51] Qianqian Wang, Zhicheng Wang, Kyle Genova, Pratul P. Srinivasan, Howard Zhou, Jonathan T. Barron, Ricardo Martin-Brualla, Noah Snaveley, and Thomas A. Funkhouser. Ibrnet: Learning multi-view image-based rendering. In *IEEE Conference on Computer Vision and Pattern Recognition, CVPR 2021, virtual, June 19-25, 2021*, pages 4690–4699. Computer Vision Foundation / IEEE, 2021. 2
- [52] Daniel Watson, William Chan, Ricardo Martin-Brualla, Jonathan Ho, Andrea Tagliasacchi, and Mohammad Norouzi. Novel view synthesis with diffusion models. In *The Eleventh International Conference on Learning Representations, ICLR 2023, Kigali, Rwanda, May 1-5, 2023*. OpenReview.net, 2023. 2, 3
- [53] Chao-Yuan Wu, Justin Johnson, Jitendra Malik, Christoph Feichtenhofer, and Georgia Gkioxari. Multiview compressive coding for 3D reconstruction. *arXiv:2301.08247*, 2023. 2, 3
- [54] Deji Xu, Yifan Jiang, Peihao Wang, Zhiwen Fan, Humphrey Shi, and Zhangyang Wang. Sinnerf: Training neural radiance fields on complex scenes from a single image. 2022. 3
- [55] Deji Xu, Yifan Jiang, Peihao Wang, Zhiwen Fan, Yi Wang, and Zhangyang Wang. Neurallift-360: Lifting an in-the-wild 2d photo to a 3d object with 360° views. 2022. 2, 3
- [56] Lior Yariv, Jiatao Gu, Yoni Kasten, and Yaron Lipman. Volume rendering of neural implicit surfaces. In *Advances in Neural Information Processing Systems 34: Annual Conference on Neural Information Processing Systems 2021, NeurIPS 2021, December 6-14, 2021, virtual*, pages 4805–4815, 2021. 2, 3
- [57] Alex Yu, Vickie Ye, Matthew Tancik, and Angjoo Kanazawa. pixelnerf: Neural radiance fields from one or few images. In *IEEE Conference on Computer Vision and Pattern Recognition, CVPR 2021, virtual, June 19-25, 2021*, pages 4578–4587. Computer Vision Foundation / IEEE, 2021. 2, 3
- [58] Wang Yu, Xuelin Qian, Jingyang Huo, Tiejun Huang, Bo Zhao, and Yanwei Fu. Pushing the limits of 3d shape generation at scale. *arXiv preprint arXiv:2306.11510*, 2023. 3
- [59] Linqi Zhou, Yilun Du, and Jiajun Wu. 3d shape generation and completion through point-voxel diffusion. In *Proceedings of the IEEE/CVF International Conference on Computer Vision*, pages 5826–5835, 2021. 3
- [60] Zhizhuo Zhou and Shubham Tulsiani. Sparsefusion: Distilling view-conditioned diffusion for 3d reconstruction. In *Proceedings of the IEEE/CVF Conference on Computer Vision and Pattern Recognition*, pages 12588–12597, 2023. 2, 3
- [61] Hao Zhu, Hao Su, Peng Wang, Xun Cao, and Ruigang Yang. View extrapolation of human body from a single image. In *Proceedings of the IEEE Conference on Computer Vision and Pattern Recognition*, pages 4450–4459, 2018. 2, 3

Consistent-1-to-3: Consistent Image to 3D View Synthesis via Geometry-aware Diffusion Models

Supplementary Material

6. Overview

In this supplementary material, we first provide the technical details of the proposed method to complement the paper. Second, we describe the experiment details, including the metric computation and reproducing baselines. Finally, we present additional qualitative results of baselines and our approach. Please see our **video** for an overview of our work and more visualizations.

7. Technical Details

Epipolar Attention. The epipolar line computation process is visualized in Fig. 8 (a). Given a point p on the image plane of the target view i and the relative camera pose $\pi^{i \rightarrow j}$, the goal is to compute the corresponding epipolar line e on the image plane of the source view j . We first compute the 3D ray of point p , then we project any two 3D points on this ray onto the source view image plane. The line connected by these two projected points is the epipolar line e .

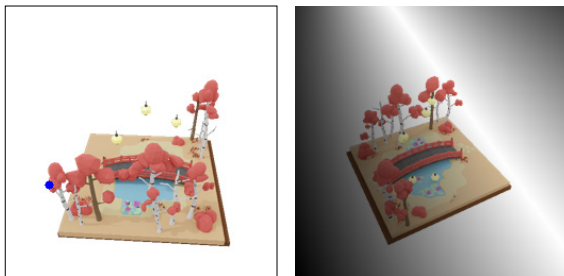
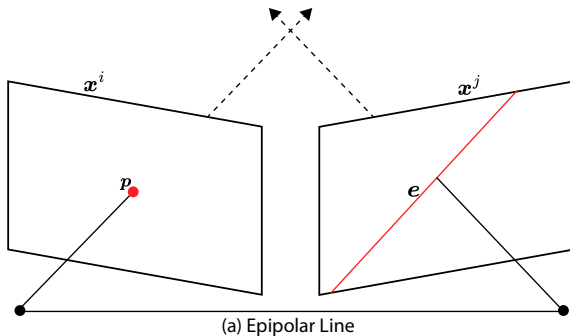


Figure 8. By combining the view-conditioned diffusion model and NeRF-style reconstruction techniques, our method is able to preform high-fidelity 3D reconstruction for any single images.

As mentioned in the main text, after getting the epipolar line, we compute pixel distances between patch centers from different views and invert it to weight map $K_{i,j}$. Finally, we directly add $K_{i,j}$ to the original attention weights $A_{i,j}$:

Parameter	Value
Input view num	1 - 4
Output view num	1 - 4
Image size	256
Latent image size (after vae)	32
SRT feature dim	768
SRT head num	12
SRT activation	gelu
SRT-Enc layer num	8
SRT-Dec layer num	4
UNet down/up block num	4
UNet block out channels	(320, 640, 1280, 1280)
UNet in channels	8
UNet out channels	4
UNet activation	silu
Diffusion steps (training)	1000
Diffusion steps (inference)	50
Sampling method	PNDM
Optimizer	AdamW
Learning rate	$5e^{-5}$
AdamW Betas	(0.9, 0.999)
Iterations	100,000
Batch Size	1024
Diffusion loss weight	1.0
Reconstruction loss weight	0.5

Table 5. We report main hyper-parameters used in our method here.

$A'_{i,j} = A_{i,j} + K_{i,j}$. In Fig. 8 (b), for the blue point in the left figure, we show its corresponding inverted epipolar distances on the right side.

UNet Block. The UNet block consists of three modules: (i) a convolution layer; (ii) a self-attention layer among multiple output views; (iii) Cross-attention layer between input views and output views. The noisy latent images y (concatenated with $\tilde{x}^{\text{target}}$ predicted by SRT) are first passed to a convolution layer to obtain patch-level image features. Secondly, instead of performing self-attention within each individual view, we merge tokens from multiple output views and apply self-attention across all these tokens. Finally, we concatenate patch tokens with the corresponding ray embedding, and apply an epipolar attention between individual output views and input tokens (obtained by SRT).

Hyper-parameters. Hyper-parameters used in our method are reported in Tab. 5.

8. Experiment Details

Dataset. We directly use the rendering data and the training/test split of the Objaverse dataset [7] provided by

Zero123 [22]. The whole dataset contains 800k objects, with 7k for testing. For each object, Zero123 provides 12 random views sampled from a uniform sphere. In addition, we employ the Google Scanned Object (GSO) dataset to evaluate the zero-shot ability of our method. For GSO, we directly use the rendering data provided by IBRNet [51]. During evaluation, we take the first frame of each object as the source frame and employ the subsequent frame as the target frame.

Metrics. We employ the VGG model, pre-trained on the ImageNet dataset, to calculate the LPIPS score. While computing the flow warping error E_{warp} , the pre-trained RAFT [47] model is used to compute the optical flow between consequent frames. For each object, a 32-frame video is generated where phi spans 360 degree, and the elevation is set to 10 degree with a radius of 1.5.

Reproducing Baselines.

- Zero123. We use the official implementation on GitHub¹ and the checkpoint pre-trained on Objaverse. We keep all the hyper-parameters and use their demo example to perform novel view synthesis. During inference, the guidance scale is set to 3.0 and the image is resized to 256×256 .
- Point-E. We use the official implementation and pre-trained models on GitHub². We follow their example demo to perform 3D reconstruction.
- PoseDiff. While the code is publicly available at the moment, we faithfully re-implement their model based on the description in the paper. All hyper-parameters are consistent with our approach.

¹<https://github.com/cvlab-columbia/zero123>

²<https://github.com/openai/point-e>